THE AMERICAN SOCIETY OF MECHANICAL ENGINEERS
345 E. 47 St., New York, N.Y. 10017

92-GT-92

The Effects of Blade Loading in Radial and Mixed Flow Turbines

H. CHEN, M. ABIDAT and N. C. BAINES
Mechanical Engineering Department
Imperial College
Exhibition Road
London SW7 2BX
UK

M. R. FIRTH
Holset Engineering Co., Ltd.
Turnbridge
Huddersfield HD1 6RD
UK

ABSTRACT

Understanding of the effects of blade loading and blade number in radial and mixed flow turbines is often based on analogies with axial turbine cascade tests or centrifugal compressors rather than direct measurement. In this paper test results from a series of similar mixed flow turbines are described. The turbine rotors differ only in blade number or inlet incidence variation. The results comprise performance data and hub and shroud pressure measurements, from which it is possible to deduce parameters such as incidence angle with good accuracy. In addition, predictions of blade loading using three-dimensional computations are shown. The results are correlated against a loading coefficient and a slip factor, both derived for the general case of a mixed flow turbine. The influence of these parameters on the performance of the tested turbines, and for comparison of other radial turbines, is shown.

NOMENCLATURE

A	flow area (m^2)
C	isentropic jet speed (m/s)
h	enthalpy (J/kg)
M	relative Mach number
$\dot{m}$	mass flow rate (kg/s)
P	pressure (N/m^2)
R	gas constant (J/kg-K)
r	radius (m)
T	temperature (K)
U	rotor peripheral speed (m/s)
V	absolute velocity (m/s)
W	relative velocity (m/s)
Z	number of the blade, axial coordinate (m)
α	angle of absolute velocity
β	angle of relative velocity
γ	ratio of specific heats
η	turbine efficiency
ψ	loading factor
μ	slip factor

Subscript

0	stagnation state
2	rotor inlet
3	rotor exit
∞	infinite blade number
b	blade
exit	turbine exit
m	meridional component
N	new definition
opt	optimum value
s	Stanitz definition
u	tangential component

INTRODUCTION

The radial turbine is recognized as an alternative to the more common axial turbine where the benefits of a simple, one-piece construction, low cost, and high specific work output are important. Long used in turbocharger applications, it is now increasingly considered for low cycle pressure ratio gas turbine engines, where a single radial stage may substitute for two axial stages (Pullen and Baines, 1992). However, a penalty is usually paid for a lower efficiency, and this is largely a reflection of the less well developed understanding and design of radial turbine rotors. In axial turbines the relationships between stage loading, flow coefficient and efficiency are based on extensive testing of many prototypes and have been well understood for many years (Ainley and Mathieson, 1957; Smith, 1965). By contrast, radial turbine development is still largely based on cut-and-try, although the advent of sophisticated measuring and computational techniques is gradually changing this (Kitson et al, 1990).

The geometric options available to the radial turbine aerodynamicist are also seriously limited by stress and materials, which almost invariably constrain the rotor inlet blade angle to be set at zero (i.e. the radial direction) to avoid any bending stress in the blades generated by centrifugal force. Attempts have been made to overcome this problem by introducing mixed flow rotors, in which the rotor inlet is a combination of radial and axial (in the meridional plane). This permits non-zero inlet blade angles to be introduced without departing from a radial blade section criterion (Cheng and Gibbs, 1989; Naguib, 1986; Yamaguchi et al, 1984; Abidat et al, 1992).

Presented at the International Gas Turbine and Aeroengine Congress and Exposition
Cologne, Germany June 1-4, 1992

In this paper we examine the loading of radial and mixed flow turbines, with the intention of understanding how changes in loading influence the performance of such machines. The analysis is based on detailed experimental measurements together with numerical studies, using turbine rotors of different blade number and inlet incidence variation across the span.

MIXED AND RADIAL FLOW TURBINES

Studies were based on data from five turbines, three mixed flow and two radial flow. The three mixed flow turbine rotors were of identical inlet and exit diameters. Turbine A had 12 blades and was designed with a camberline such that the inlet blade angle was constant at 20° across the span. Due to the changing radius across the span and the vortex flow created by the turbine stator, this implies that the angle of incidence is not constant at all positions. Turbine B had the same blade number, but the camberline was redesigned to give a notionally constant incidence (assuming that the stator exit flow was a free vortex), and the rotor has a reduced axial length. The blade angle at the mean inlet radius was kept at 20°. Turbine C was identical to turbine A except that the blade number was reduced to 10.

The two radial turbine rotors, D and E, were commercial designs, of similar size to the mixed flow rotors. Both had 12 blades. For detailed information about all five turbines, see Abidat (1991) and Chen (1990).

The turbines were tested in flow rigs to measure the performance over a wide range of operating conditions. The rigs run on cold air and use a centrifugal compressor as the loading device. The turbine power output is measured by the sum of the compressor air temperature rise and the heat rejected in the bearings. Additionally, for turbines A-C only, extensive wall static pressure measurements were made. Fourteen pressure tappings were located on the shroud, four upstream of the blade leading edge, eight distributed along the blade passage, and two downstream (Fig. 1). Additionally four tappings were used to measure the hub pressure upstream of the blade. A full description of the experimental data including exit traverses, is given by Abidat et al (1992) and Chen et al (1991).

NUMERICAL AND ANALYTICAL METHODS

Using the data from experiment, numerical simulation was carried out to study the 3-D flow within the blade rows. First a one-dimensional off-design program (Chen and Winterbone, 1990) was run, which generated the mean flow condition at the turbine casing. This mean condition can then be used as upstream boundary conditions for a 3-D program. The program uses flux-vector splitting, finite volume technique to solve 3-D inviscid Euler equations in the blade rows. A computational grid is extended both upstream and downstream the blade. The upstream extension simulates the flow inside the turbine casing, and is thought to give more correct flow conditions at the blade leading edge than simply put a straight extension upstream of the blade row. With the upstream conditions given by above method, the 3-D program usually gave correct mass flow prediction. The simulation was carried out at the points of peak efficiency, which correspond to pressure ratio = 2.55 for turbine A, 2.53 for B and 2.56 for C.

The test data were also used in a 1-D model to calculate flow conditions at the rotor inlets. That is, measured mass flow rate, stagnation pressure and temperature at the turbine inlets were used in conjunction with free-vortex and isentropic flow assumptions, to obtain the mean flow conditions at the inlets of the rotors. A more complicated 1-D model (Chen, 1990) was used for turbine E.

RESULTS AND DISCUSSION

Measured performance of turbines A and C are shown in Figures 2-3. There is a about 2% penalty in peak total-to-static efficiency at design speed due to the reduction of blade number. The peak efficiency of turbine A occurs at higher blade-jet speed ratio U_2/C than that of turbine C. The increase of U_2/C value is due to the increase in turbine A efficiency and decrease of its loading factor The reduction in turbine efficiency is discussed later. Turbine C has a larger swallowing capacity than turbine A, a direct result from reduced blade blockage. The difference is about 1.6% at the design point (pressure ratio = 2.9).

The shroud pressure distributions measured on rotors A and C at 100% speed and two pressure ratios are shown in Fig. 4. It appears that turbine A may suffer a more severe incidence at shroud, with the shroud pressure holding nearly constant immediately after the blade leading edge. This is consistent with the fact that turbine A has more blades so that its optimum relative flow angle is not as negative as that of turbine C. (Turbine A was designed to achieve optimum incidence at mean radius. This means that at the shroud, a departure from the optimum value occurs). As the fluid went further down the blades, it expanded smoothly in both rotors, but rather more so in rotor A. In rotor C the fluid first expanded rapidly as it entered the blades, accompanied by a sharp drop in the shroud pressure, and then the pressure held nearly constant with little acceleration indicated also by velocity distributions at the shroud. As diffusions may result in flow separation, it seems that some flow separation may have occurred in turbine C, judging from its efficiency and Fig. 4. Turbine A also has a higher shroud pressure than C for the most part of the blade passage, as indicated in the figure.

The measured shroud and hub pressures at blade leading edge are shown for the two turbines in Figures 5-8. They reveal that there was a large pressure gradient across the rotor inlets, with higher pressure occurring at the shroud. This pressure gradient is necessary to balance the difference in centrifugal force between the shroud and hub, resulting from the change of radius. This suggests that any design procedure of mixed flow turbines with low hub- to tip-radius ratio should take this radial change of inlet condition into account. The conditions here may be compared with the design practice of axial flow turbines, where a hub- to tip-radius ratio 0.85 is considered as a criterion (Glassman et al, 1975). The changes in shroud and hub pressures with overall pressure ratio and speed are also interesting. Although the shroud pressure varied almost linearly with the overall pressure ratio, the hub pressure was rather a parabolic function of the pressure ratio. At low speeds there was a point when a decrease in the pressure ratio from that point resulted in an increases in the hub pressure. For turbine C this trend was very clear, and began to occur at higher speeds. How these patterns related to the velocity field at the rotor inlets is not very clear at this stage.

The blade loading is directly affected by blade number. In the case of axial flow turbines, the loading is widely assessed by Zweifel coefficient which relates an actual blade loading to an ideal blade loading. For radial and mixed flow rotors, because there is a radius change from their inlet to exit, a similar relation

becomes complicated and is not very meaningful. Another coefficient also used in the situation of axial flow turbines is so-called loading factor or loading coefficient (Glassman et al, 1975)

$$\psi = \Delta h_0 / U_2^2 \qquad (1)$$

where Δh_0 is the total enthalpy drop across rotors. So the loading factor is the ratio of energy developed by the rotor to rotor kinetic energy, or dynamic condition of the rotor. Using the Euler equation for turbomachines

$$\Delta h_0 = U_2 V_{u,2} - U_3 V_{u,3} \qquad (2)$$

leads to

$$\psi = (V_u/U)_2 - (r_3/r_2)(V_{u,3}/U_2) \qquad (3)$$

Since we are here concerned with the design condition of turbines, the second term in above equation is relatively small and can be neglected. This gives the following simplification

$$\psi = (V_u/U)_2 \qquad (4)$$

So the loading factor is not only a application parameter which expresses the requirements of application, but also a velocity diagram parameter. A comparison of this loading factor is given in Fig. 9 for three mixed flow turbines and one radial flow turbine at their design speeds. Turbine C has consistently higher values of ψ than A over the entire operating range. Turbine B, which has a shorter rotor, also shows higher ψ. The curves in Fig. 9 indicate that there is a maximum value of ψ for the each turbine, which is slightly larger than 1 for turbines B and C, and close to 1 for turbine A and 0.95 for D. Further increase pressure ratio beyond this point does not increase the value of ψ. These features suggest that ψ, expressed by equation (4), can be used as a practical design parameter. And ψ = 1 indicates a design criterion for this kind of turbines.

Figures 10-12 further show the blade loading diagrams of turbines A and C, at shroud, mid-span and hub sections, using the 3-D inviscid flow simulation. Both turbines suffered a negative loading at inlet, especially at the shroud. This is due to large negative incidence encountered at that region. As a whole, however, both turbines show very good loading pattern. This may explain their high efficiency. Again the figures show that turbine C has higher loading than turbine A.

SLIP FACTOR

One of the effects that blade number has on turbine performance is that it influences the optimum flow angle or the slip at rotor inlet, which is usually quantified by a slip factor taking the form of (Whitfield and Baines, 1990)

$$\mu = 1 - \frac{V_{2u,\infty} - V_{2u}}{U_2} \qquad (5)$$

where $V_{2u,\infty}$ is the tangential component of absolute velocity when the slip does not occur or the flow is perfectly guided by the blades (Fig. 13a). From it the loading factor ψ can be related to the slip factor by

$$(V_u/U)_2 = \frac{\mu}{1 - \frac{\tan\beta_{2b}}{\tan\alpha_2}} \qquad (6)$$

There are many theoretical solutions of the slip factor based on the 2-D potential flow theory in centrifugal compressors, and they have been applied directly to radial and mixed flow turbines. The one most commonly used was given by Stanitz (1952)

$$\mu_s = (V_u/U)_{2,opt} = 1 - 0.63\pi/Z \qquad (7)$$

where Z is the blade number. The Stanitz equation gives the optimum value of V_{2u}/U_2 for a particular rotor, and at this optimum value, the flow is supposed to enter the rotor blades smoothly without producing extra losses. By checking the values of the loading coefficient given by equation (6) and the Stanitz equation and those deduced from the experimental data of the turbines studied here, it was found that at their peak efficiency points, the three mixed flow turbines have values of ψ ranging from 0.952 to 0.967 (Fig. 9), but the values predicted by equation (6) and the Stanitz correlation are 0.937 for turbines A and B, and 0.900 for turbine C. The trend of the change of blade loading with blade number is incorrectly predicted. Given the fact that ψ expresses the blade loading, one would naturally expect it should reduce with increase of the blade surface or the blade number. For radial turbines D and E, the loading coefficients deduced from the test data are 0.924 (Fig. 9) and 0.946, again different compared to the fixed value of 0.835 by the Stanitz correlation. These facts call into question the applicability of the Stanitz equation (and many other expressions for the slip factor) to radial and mixed flow turbines. A recent 3-D numerical study by the authors suggests that the 3-D method can produce values of the loading factor in better agreement with the experiment.

The isentropic assumption used in the calculation for the tested turbines may produce larger ψ and thus accounts for the difference between those deduced from the test and the Stanitz equation. However, the free-vortex assumption used to calculate V_u may, on the other hand, underestimate V_u. This assumption is held under the condition of balanced tangential forces, and at the blade leading edge, unbalanced pressure forces act on the blade pressure and suction surfaces. Under subsonic inflow circumstances this pressure difference will influence the incoming flow, forcing it to turn an angle in the direction of the pressure gradient, or the rotation. This is similar to the flow turning at the leading edge of cascades or stators. Fig. 14 shows the difference in calculated relative flow angle upstream of rotors A, C and D by the free-vortex theory and by a 3-D simulation. The sudden turning of the flow at the leading edge region can be clearly seen.

There is an implicit assumption in Fig. 13a that the angle of absolute velocity varies because of the slip. Taking $V_{2u,\infty} = U_2$ and using the data of Fig. 9, the change of absolute flow angle was evaluated at the peak efficiency point of turbine D. It turned out that $\alpha_{2,\infty} - \alpha_2 = 72.66 - 68.63 = 4.03^\circ$. This value, compared with the value of 2.85° of maximum change of the angle generated by the changes of turbine operation conditions during the test, is clearly unrealistic. All the other four turbines showed similar results. There

is another problem associated with the assumption. In the view of an observer travelling with the absolute flow, slip occurs due to the downstream influence of the rotor; although in subsonic flows the downstream condition can influence the upstream conditions, in supersonic flows, it cannot. So the assumption will finally lead to the conclusion that there is no slip in supersonic flows. This, of course, cannot be justified. Fig. 13a is a direct analogy with the one used for centrifugal compressors. A similar assumption may, however, be justified there because the slip now happens upstream.

A new interpretation of the influence of the slip is proposed in Fig. 13b. It is now assumed that the absolute velocity is not affected by the slip. Instead because of the slip, the out flow from a turbine casing will embark on the rotor seemingly with a smaller rotating speed than its blade speed. In other words, because of the slip, the rotor must be larger or run at higher speeds in order to deliver the required work. In practice it does not, and so the delivered work is lower than would be expected with no slip.

It is necessary to introduce a new slip factor, defined by

$$\mu_N = 1 - \frac{U_{2\infty}}{U_2} \qquad (8)$$

The following expression can be obtained from Fig. 13b

$$\mu_N = \frac{\tan\beta_{2b} - \tan\beta_2}{\tan\alpha_2} \frac{\nabla_{2u}}{U_2} = \frac{\tan\beta_{2b} - \tan\beta_2}{\tan\alpha_2} \psi \qquad (9)$$

So in the area of interest ($\beta_2 - \beta_{2b} \leq 0$), $0 \leq \mu_N \leq 1$. μ_N is directly linked to μ defined by equation (5): from velocity triangle relation

$$\tan\beta_2 = \frac{\psi - 1}{\psi} \tan\alpha_2$$

equation (9) can be written as

$$\mu_N = 1 - \psi + \frac{\tan\beta_{2b}}{\tan\alpha_2} \psi = 1 - \mu \qquad (10)$$

So all the correlations developed for μ are also applicable to μ_N. However, the difficulties encountered by μ, the change of absolute flow angle and supersonic conditions, is avoided.

CONCLUSIONS

(1) Reducing the blade number of mixed-flow turbine A from 12 to 10 leads to higher blade loading and results in about a 2% efficiency penalty. It also results in a flatter efficiency characteristic and a higher mass flow rate.

(2) The higher blade loading of turbine C is accompanied by stronger diffusion. This increases the possibility of flow separation and loss.

(3) The large change of rotor inlet conditions with radius and poor flow conditions at the hub sections indicate the sensitivity of selecting the inlet conditions at the mean section.

(4) The loading of the five turbines studied here can be judged from their loading factor ψ, equation (4). $\psi = 1$ appears to be a criterion for both radial and mixed flow turbines.

(5) A new interpretation of the slip is proposed. It overcomes the difficulties from the traditional interpretation. And if free-vortex theory is used to obtained the rotor inlet conditions the slip should be considered to be composed of a turning slip and a rotation slip, the former partly cancels the effect of the latter.

REFERENCES

Abidat M. Design and testing of a highly loaded mixed flow turbine. Ph.D. thesis, Imperial College, University of London, 1991.

Abidat M, Chen H, Baines N C and Firth M R. Design of a highly loaded mixed flow turbine. To be published, Proc. Inst. Mech. Engrs. Journ. Power and Energy, 1992.

Ainley D G and Mathieson G C R. A method of performance estimation for axial flow turbines. Aero. Res. Coun. Reports and Memoranda 2974, 1957.

Chen H. Steady and unsteady performance of vaneless casing radial inflow turbines. Ph.D. thesis, UMIST, 1990.

Chen H. and Winterbone D E. A method to predict performance of vaneless radial turbines under steady and unsteady flow conditions. In Turbocharging and Turbochargers, Inst. Mech. Engrs., pp. 13-22, 1990.

Chen H., Abidat M, Baines N C and Firth M R. Exit traverse of mixed flow turbines with inlet incidence variation. Internal Report, Mech. Eng. Dept., Imperial College, 1991.

Cheng C C and Gibbs C A. The design and testing of a mixed flow turbine for turbochargers. SAE Paper 890644, 1989.

Glassman A J et al. Turbine design and application. NASA SP-290.

Kitson S T, Maguire J M, Langdon P J, Varo R G and Shaw G D. The computational experiment applied to aerodynamic design and analysis of turbomachinery. SAE Paper 900360, 1990.

Naguib M. Experience with the modern RR151 turbocharger for high-speed diesel engines. In Turbocharging and Turbochargers, Inst. Mech. Engrs., pp. 105-112, 1986.

Pullen K R, Baines N C and Hill S H. The design and evaluation of a high pressure ratio radial turbine. To be presented, ASME Gas Turbine Conference, Cologne, 1992.

Smith S F. A simple correlation of turbine efficiency. J. Royal. Aero. Soc. Vol 69, p 467, 1965.

Stanitz J D. Some theoretical aerodynamic investigations of impellers in radial- and mixed-flow centrifugal compressors. ASME Trans., Vol. 74, No. 4, May 1952, pp. 473-497.

Whitfield A. and Baines N C. Design of radial turbomachines. Longman Scientific & Technical, 1990, England.

7 Yamaguchi H, Nishiyame T, Horlai K and Kasuya T. High performance Komatsu KTR 150 turbocharger. SAE Paper 840019, 1984.

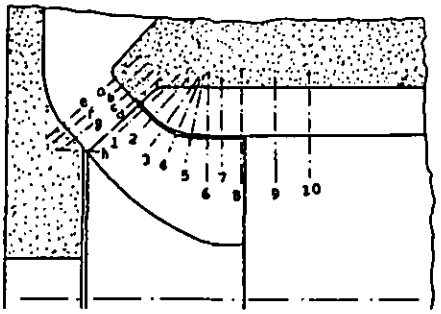

Fig. 1 Wall pressure tapping layout

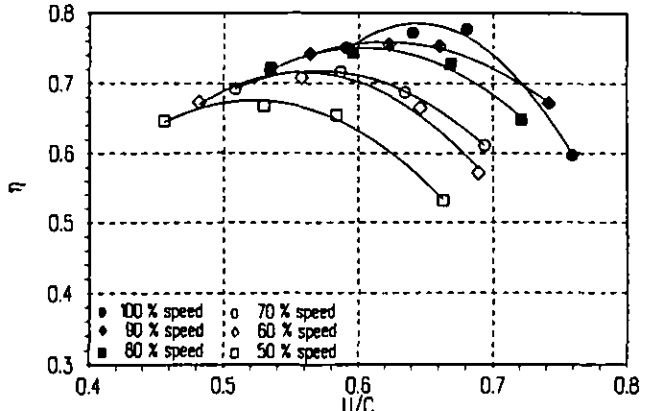

Fig. 2 Total-to-static efficiency of turbine A

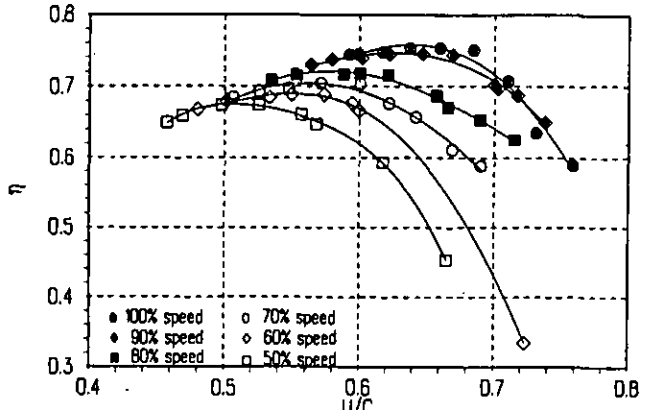

Fig. 3 Total-to-static efficiency of turbine C

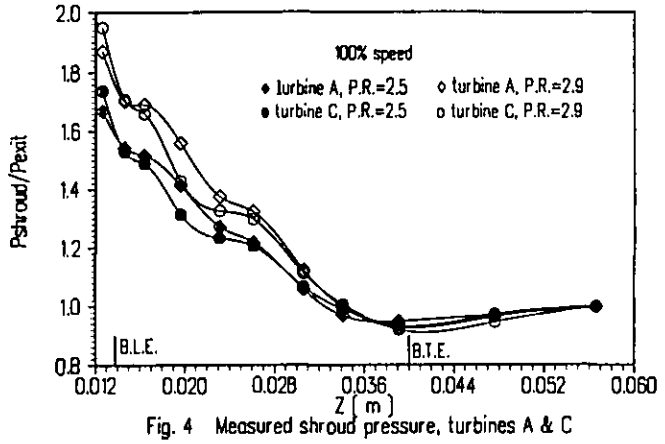

Fig. 4 Measured shroud pressure, turbines A & C

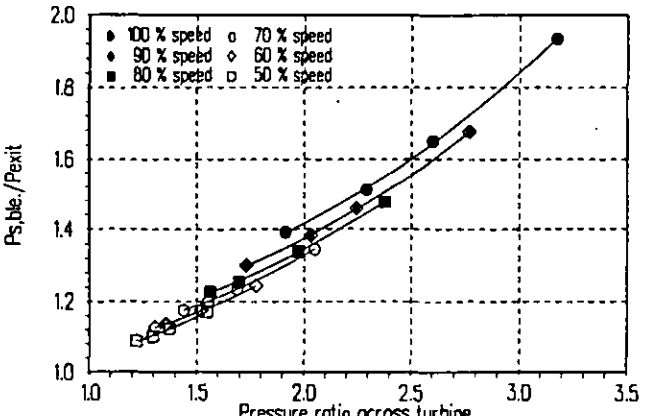

Fig. 5 Shroud pressure at B.L.E. of turbine A

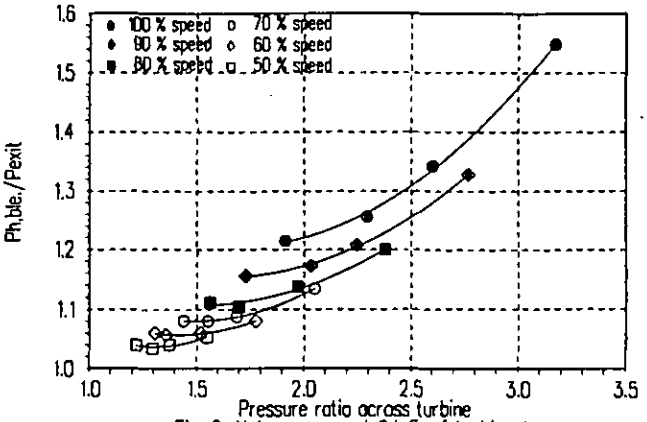

Fig. 6 Hub pressure at B.L.E. of turbine A

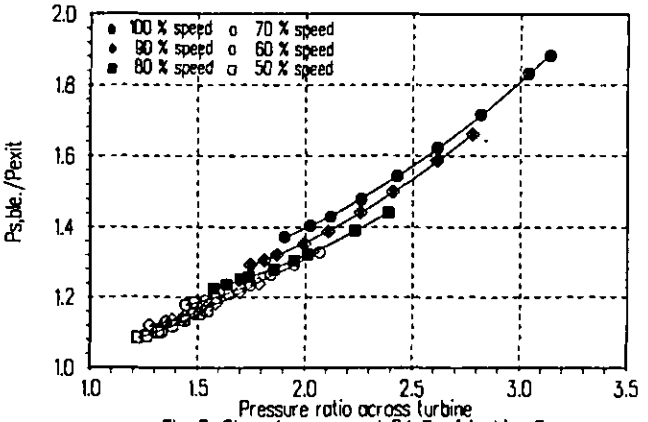

Fig. 7 Shroud pressure at B.L.E. of turbine C

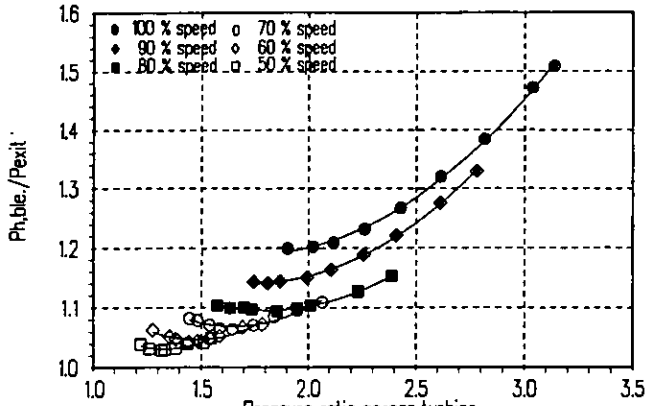

Fig. 8 Hub pressure at B.L.E. of turbine C

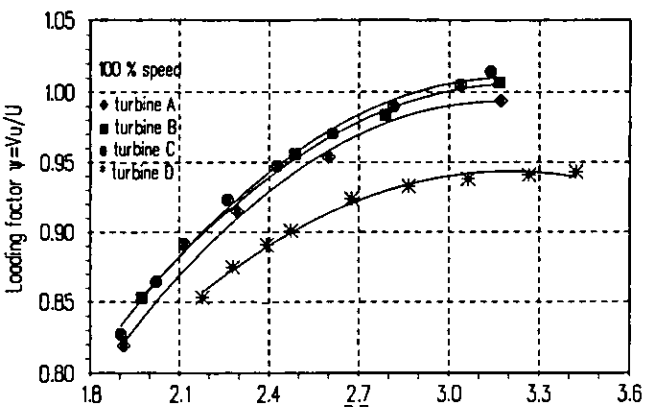

Fig. 9 Loading factor of radial & mixed turbines

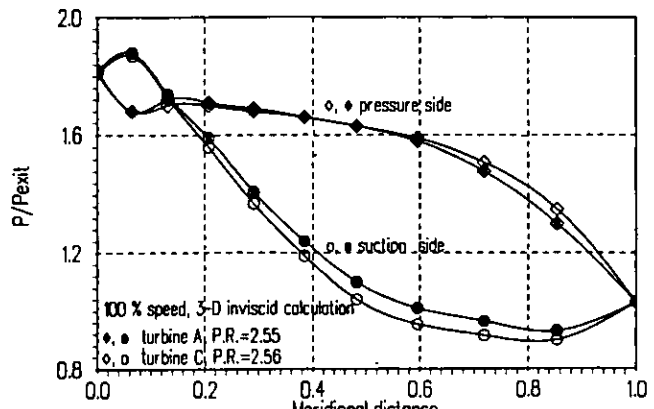

Fig. 10 Calculated blade loading at shroud, A & C

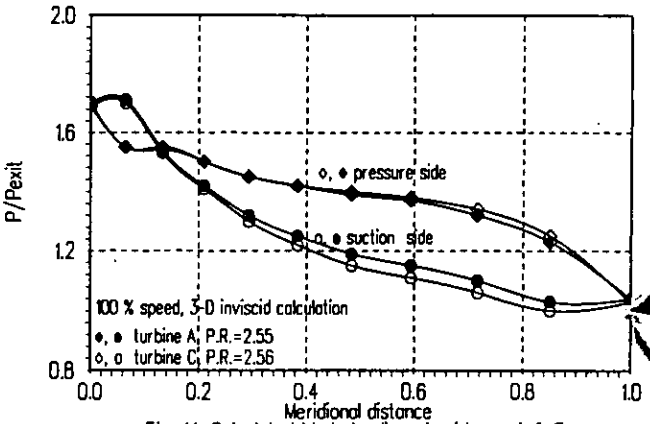

Fig. 11 Calculated blade loading at midspan-A & C

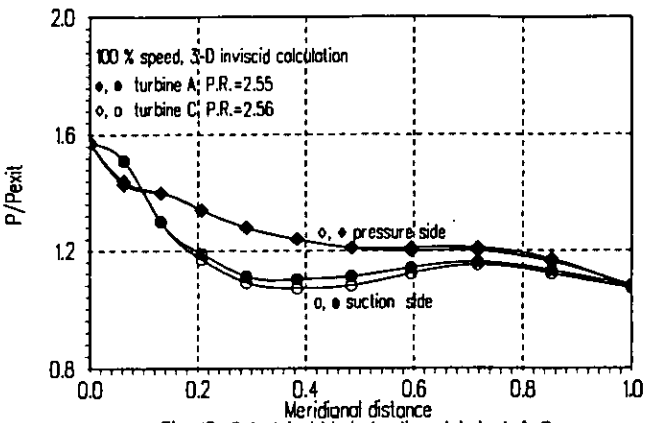

Fig. 12 Calculated blade loading at hub, A & C

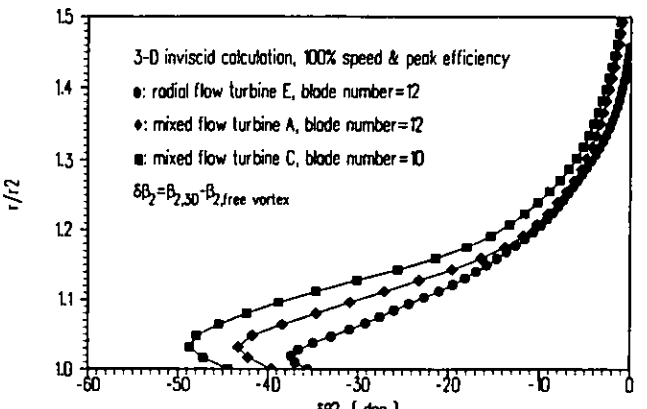

Fig. 14 Deviation of β2 from free vortex theory

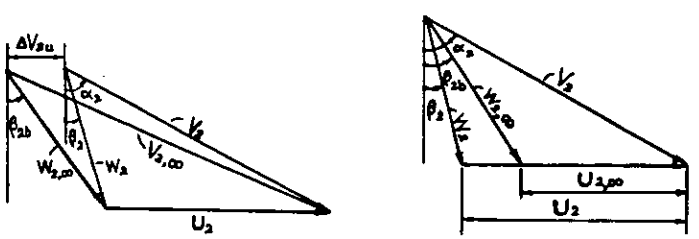

(a) V_{2m}: constant; α_2: varies (b) V_{2m}: constant; α_2: constant

Fig. 13 The slip and Velocity triangles